

Isotopic water separation using AGMD and VEMD

Jaewoo Kim,
Sang Eon Park,
Taek-Soo Kim,
Do-Young Jeong,
Kwang-Hoon Ko

Abstract The ^{18}O isotopic water permeation and separation characteristics of a hydrophobic PTFE membrane using Air Gap Membrane Distillation (AGMD) and Vacuum Enhanced Membrane Distillation (VEMD) were investigated. Permeation fluxes were measured by weighing the collected membrane-permeated water vapor. $^{18}\text{O}/^{16}\text{O}$ of each water sample was analyzed by the Tunable Diode Laser Absorption Spectroscopy (TDLAS). We observed the effects of the air filled membrane pores and the temperature gradient applied to the membrane surfaces on the vapor permeation flux and the oxygen isotope separation for the first time. For both AGMD and VEMD, the permeation flux and the degree of ^{18}O separation increased as the membrane interfacial temperature gradient increased. Even though, oxygen isotope separation and the permeation flux for VEMD is slightly higher than AGMD, the latter may be more efficient from the system's operational point of view.

Key words AGMD • VEMD • oxygen isotopes • PET • FDG

Introduction

Enriched stable isotopes in the modern era are essential as the demand and applications for them in medicine, industry, and science increase and expand significantly. Especially, ^{18}O -enriched water (> 90%) is used as a target in the cyclotron for the production of the β -emitting radioisotope ^{18}F , which is essential for PET (Positron Emission Tomography) pharmaceutical [^{18}F]-labeled 2-deoxyglucose (FDG) synthesis. Currently, ^{18}O is produced by cold distillation of NO (nitric oxide) or fractional distillation of water. These processes, however, are technically complicated and costly so as to limit the production of ^{18}O . In this regard, membrane distillation (MD) has been investigated for many years as a promising ^{18}O separation process.

Oxygen isotope separation using polymeric membranes were firstly observed by Chmielewski *et al.* in the early 90's [9]. Separations of oxygen and hydrogen isotopes were investigated by using the Pervaporation, Air Gap Membrane Distillation (AGMD), and Direct Contact Membrane Distillation (DCMD) of water [1–4]. MD utilizes the differential diffusivity of the water vapor in the membrane pores owing to their isotopic mass differences. However, the effects of air already filled in the membrane pores and the roles of the temperature gradient applied to the membrane surfaces on the isotopic diffusion characteristics have not been experimentally investigated.

MD can be described well by the diffusion of the water vapor with a mean free path λ through the membrane pores. The mean free path of a water molecule, in general, can be expressed as $\lambda = kT/(\sqrt{2}\pi\sigma^2P)$, where: $k = (1.38 \times 10^{-23} \text{ J/K})$

J. Kim[✉], T.-S. Kim, D.-Y. Jeong, K.-H. Ko
Laboratorium for Quantum Optics,
Korea Atomic Energy Research Institute,
Dukjin-Dong 150, Yusung-Gu, Daejeon, Korea 305-353,
Tel.: 82 42 868 8931, Fax: 82 42 868 8576,
e-mail: kimj@kaeri.re.kr

S. E. Park
Division of Metrology,
Korea Research Institute of Standards and Science,
Doryong-Dong 1, Yusung-Gu, Daejeon, Korea 305-340

Received: 29 March 2004, Accepted: 4 August 2004

is the Boltzman constant; σ is a collision diameter ($\sim 2.7 \text{ \AA}$ for a water molecule); T is the temperature, and P is the vapor pressure. For example, λ of the water molecules at 40°C and 60°C are 1.8 \mu m and 0.7 \mu m , respectively, when there are no air molecules in the membrane pores. For the flow of the water vapor in the ideal cylindrical pores, it is reasonable to consider a Knudsen diffusion if λ is bigger than the pore diameter, while a molecular diffusion is suitable for a smaller λ when the air is present in the pores. Hence, the flow of the water vapor under 60°C through the sub-micro porous membrane is assumed to be the Knudsen flow type in the absence of air in the pores. If air is already filled in the sub-micro pores, however, the flow of the water vapor should be treated as a molecular flow at the same temperature region. It is clear that the membrane permeation flux of the water vapor is strongly dependent on the water temperature, because it determines the pressure of the water vapor in the pores. In addition to this, the geometric membrane pore properties and the temperature gradient applied to the membrane surfaces are important to estimate the isotopic diffusion effects. For AGMD, the membrane-permeated water vapor is collected on the heat exchange surface after diffusing through the air in the membrane pores. On the other hand, air does not exist in the permeation cell for ideal VEMD. Evidently, the water vapor diffuses through the free space in membrane pores.

In this investigation, we carried out the AGMD and VEMD experiments under various temperature conditions observing the effects of the pore air and the membrane interfacial temperature gradient. The ^{16}O and ^{18}O isotopic concentrations of the water samples were measured by the Tunable Diode Laser Absorption Spectroscopy (TDLAS). TDLAS compares the ro-vibrational absorption peak ratios of the $\nu_1 + \nu_3$ (around 1.392 \mu m) vibrational combination band of a water molecule [5, 6, 8].

Material and methods

Experimental system and procedure

Figure 1 shows a schematic diagram of the MD system which consists of a membrane permeation cell, a temperature controlled water circulation system, and sample collection traps. The hydrophobic PTFE porous membrane (Millipore FGLP, Fig. 2) with the effective area of 12.56 cm^2 in the permeation cell was supported by a stainless steel grid. A membrane with the average pore diameter of 0.2 \mu m , thickness $\sim 150 \text{ \mu m}$, porosity $\sim 70\%$, and tortuosity factor ~ 2 was tested for the permeation flux and isotope separation. Also, membranes with 0.1 \mu m , 0.45 \mu m , and 1.0 \mu m average pore diameters were experimented to check the variances of the permeation flux by the pore sizes. Water was de-ionized prior to the experiments to exclude the ion effects. The water flask was submerged in a heat bath filled with ethylene glycol, and circulated by a peristaltic pump at a fixed flow rate. The permeated water vapor was collected in the trap through a stainless steel heat exchange funnel and was weighed by a micro-scale with two decimal points. Temperatures of the flowing water and heat exchange funnel were measured with a 0.1°C resolution at the cell water inlet/outlet and at the funnel surface, respectively.

For AGMD, water temperature and pore diameter dependent permeation fluxes were investigated with and without a heat exchange funnel temperature control. Sample collection times were more than 6 hours for all the cases. VEMD was carried out under the same experimental conditions as the AGMD experiments. Samples were collected during 1 hour or shorter in the cold trap for these experiments. Heat exchange funnel temperatures were controlled at 15°C , 20°C , and 25°C by circulating the temperature controlled cold water using a chiller.

Isotopic analysis with TDLAS

$\text{H}_2^{18}\text{O}/\text{H}_2^{16}\text{O}$ of the samples were analyzed by the TDLAS system [5]. The Littman external cavity tunable diode laser (Sacher, Model TEC500-1380) producing wavelengths centered at 1.392 \mu m with a power of $\sim 3 \text{ mW}$ was used. To increase the vapor absorption signals, a multi-pass cell (Newfocus, Model 5611) whose path length is 36 m was used. A lock-in-amplifier (Stanford Research Systems, Model SR850) was employed to increase the S/N ratio of the 1st harmonic absorption signals. Peak-to-peak ratios of each isotopic 1st harmonic signal in the samples were compared to determine the change of the ^{18}O concentrations. The reference and the permeated water samples were scanned at the vapor pressure of 7 torr alternatively. Each sample was scanned more than 40 times and averaged. To acquire reliable peak-to-peak ratios, these steps were repeated several times and averaged again. The obtained signals were managed and stored by the Agilent Vee program

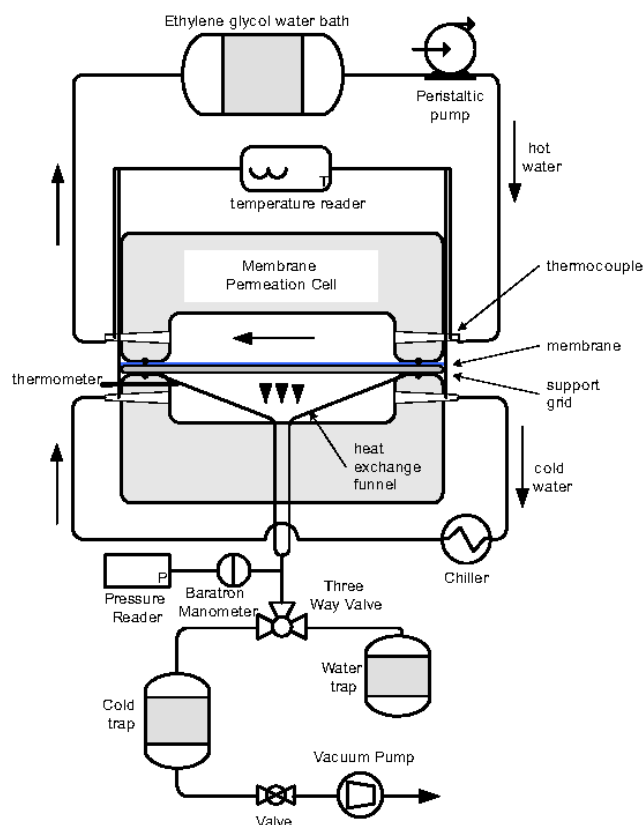


Fig. 1. Schematic diagram of the AGMD and VEMD system for oxygen isotope separation.

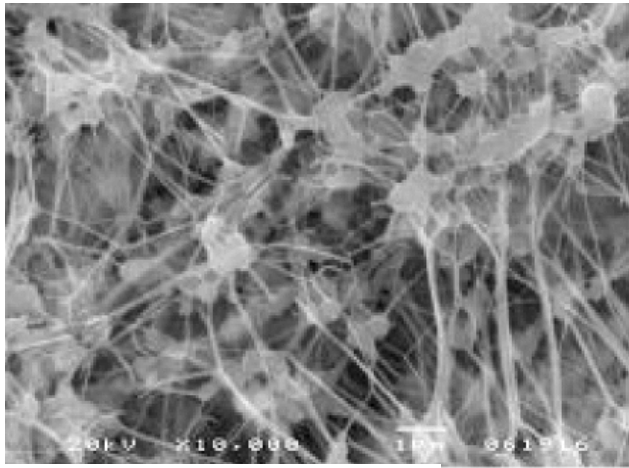
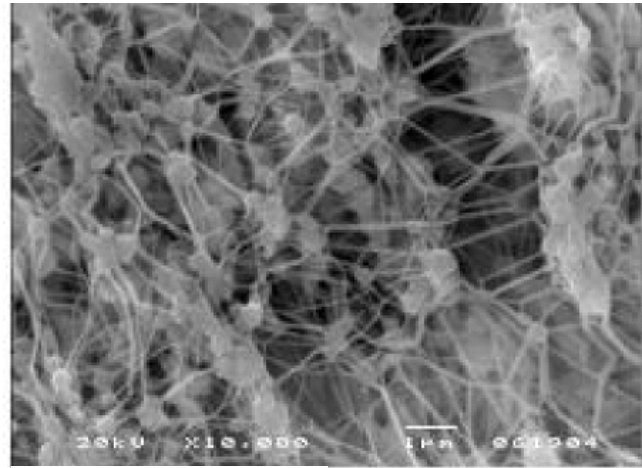
 $r_p = 0.2 \mu\text{m}$  $r_p = 1.0 \mu\text{m}$

Fig. 2. SEM (Scanning Electron Microscope) image of the hydrophobic PTFE membranes with 0.2 μm and 1.0 μm pores on average.

and the isotope separation coefficients were calculated using the Beer-Lambert Law. The ^{18}O isotope separation coefficient, in general, is defined by $\alpha = (x/(1-x))_{\text{reference}} / (x/(1-x))_{\text{permeated}}$, where x is a concentration of ^{18}O in each sample. If the laser absorption signals are used, it can be defined by the ratio of the line intensity, $I(v) = I_0 \cdot \exp[-S(T)g(v-v_0)nl]$, of H_2^{18}O and H_2^{16}O . Here: I_0 and $I(v)$ are laser beam intensities before and after absorption; $S(T)$ is the line strength; $g(v-v_0)$ is the line-shape function centered on v_0 ; n is the number density and l is the optical path length. Since the temperatures of each sample during the scanning were maintained the same, $S(T)$ and $g(v-v_0)$ cancel each other out. The ^{18}O separation coefficient, therefore, can be expressed by the ratio of the measured line intensity, $\alpha = (a_i/a_{16})_{\text{reference}} / (a_i/a_{16})_{\text{permeated}}$, where $a = \ln[I(v)/I_0]$ and i indicates ^{18}O .

Figure 3 shows the laser beam absorption signal of the water vapor measured in the oscilloscope and the 1st harmonic absorption signals processed in the lock-in-amplifier. While the S/N ratio of the absorption signal in the oscilloscope was ~ 100 , the S/N ratio of the 1st harmonic signal in the lock-in-amplifier was enhanced to ~ 1000 thus increasing the measurement accuracy. Isotopic concentra-

tions in the water samples were determined by comparing the peak-to-peak ratio of each isotope assigned in the 1st harmonic signals. Degree of the ^{18}O isotope separation was expressed by $\delta^{18}\text{O}[\text{‰}]$ representing a change of 1/1000 in the isotopic concentrations. The isotope separation coefficient, therefore, is equal to $\alpha = 1 - \delta^{18}\text{O}[\text{‰}]/1000$.

Results and discussions

Membrane permeation fluxes of the water vapor

For AGMD, the membrane permeation fluxes of the water vapor were not varied by the pore sizes at each flowing water temperature when the heat exchange funnel was not cooled as shown in Fig. 4a. Temperature differences between the flowing water (T_w) and the heat exchange funnel (T_h) in this case were $\Delta T = T_w - T_h \sim 4^\circ\text{C}$ for $T_w = 40^\circ\text{C}$ and $\Delta T \sim 6^\circ\text{C}$ for $T_w = 60^\circ\text{C}$. Based on these results, we can conclude that the permeation flux may not depend on the membrane pore size, rather it is related to the membrane porosity, which are 70% for the 0.2 μm membrane and 85% for all other membranes based on the manufacturer's information, and the water temperature. Figure 4b indicates that the permeation flux for AGMD increases as the temperature gradient applied to the membrane surface increases. Since the equilibrium vapor pressure of the water increases as the temperature of the water increases, the pressure gradient applied to the membrane surface will also be increased as the temperature gradient of the membrane surface increases. This will obviously cause a higher permeation flux. Permeation fluxes for both AGMD and VEMD without funnel cooling as shown in Fig. 4c increased as the temperature of the water increased, the same as in Fig. 4a. The flux for VEMD especially increased as much as four times compare to AGMD at the same water temperature. This may be caused by the forcibly increased pressure gradient for VEMD. This indicates that it is important to increase the water temperature and the membrane interfacial temperature gradient to increase the permeation flux for AGMD. Also a dramatic increase of the permeation flux can be obtained by applying a forcible pressure gradient to the membrane surface by using

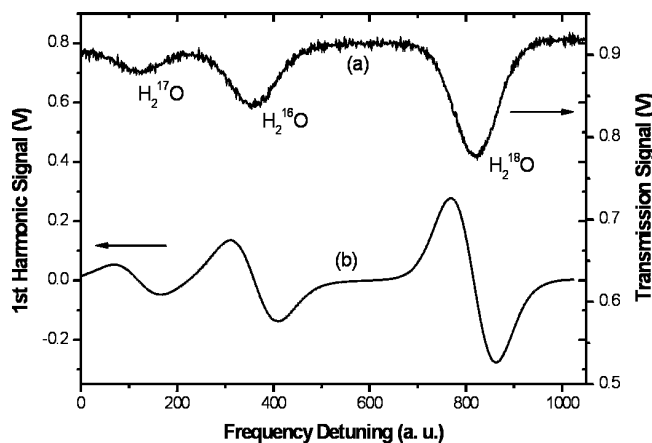


Fig. 3. Direct water vapor absorption signals from (a) the oscilloscope and the 1st harmonic signals from (b) the lock-in amplifier of H_2^{16}O , H_2^{17}O , and H_2^{18}O .

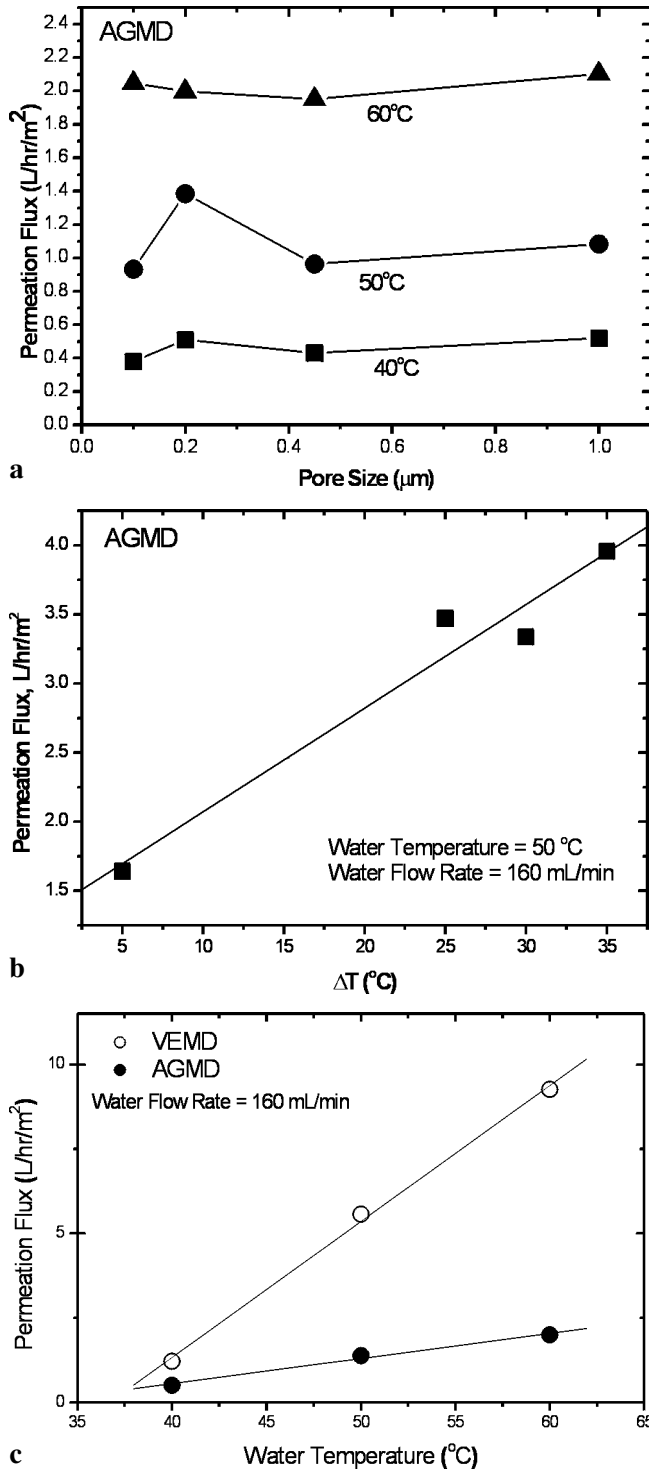


Fig. 4. Water vapor permeation properties of a hydrophobic PTFE membrane. a – Membrane pore size dependent permeation fluxes for AGMD without heat exchange funnel cooling; b – membrane interfacial temperature gradient dependent permeation flux for AGMD; c – water temperature dependent permeation flux for AGMD and VEMD without heat exchange funnel cooling.

VEMD. However, it is also important to find the optimum temperature and pressure conditions since these factors are related to the degree of oxygen isotope separation and more importantly to the capital cost and the energy expenditure for the MD system operation.

Degrees of oxygen isotope separation

Degrees of oxygen isotope separation for AGMD and VEMD are expressed by the changes of the oxygen isotopic concentrations in each sample using the unit of permil [‰]. Each data point in the graphs was obtained by averaging more than 40 scans of the H₂¹⁸O/H₂¹⁶O ratios of the permeated and reference water samples, respectively. As shown in Fig. 5a and 5b, isotope separation coefficients are 1.0044, 1.0072, and 1.0075 at T_w = 40°C, 50°C, and 60°C respectively for AGMD, and 1.0067, 1.0102, and 1.0072 at T_w = 40°C, 50°C, and 60°C respectively for VEMD when the heat exchange funnel was not cooled. Figure 6 shows the separation degrees of the oxygen isotopes for (a) AGMD and (b) VEMD at T_w = 50°C when the higher temperature gradient is applied to the membrane surfaces by the heat exchange funnel cooling. Isotope separation coefficients are 1.0074, 1.0107, 1.0125, and 1.0133 for ΔT = 5°C (no funnel cooling), 25°C, 30°C, 35°C, respectively for AGMD, and 1.0102 and 1.0144 for ΔT = 5°C (no funnel cooling) and 30°C, respectively for VEMD.

The isotope separation phenomenon of MD is relatively well explained by the characteristics of the water vapor diffusion through the ideal cylindrical membrane pores, even though the PTFE membrane pores are not ideal as

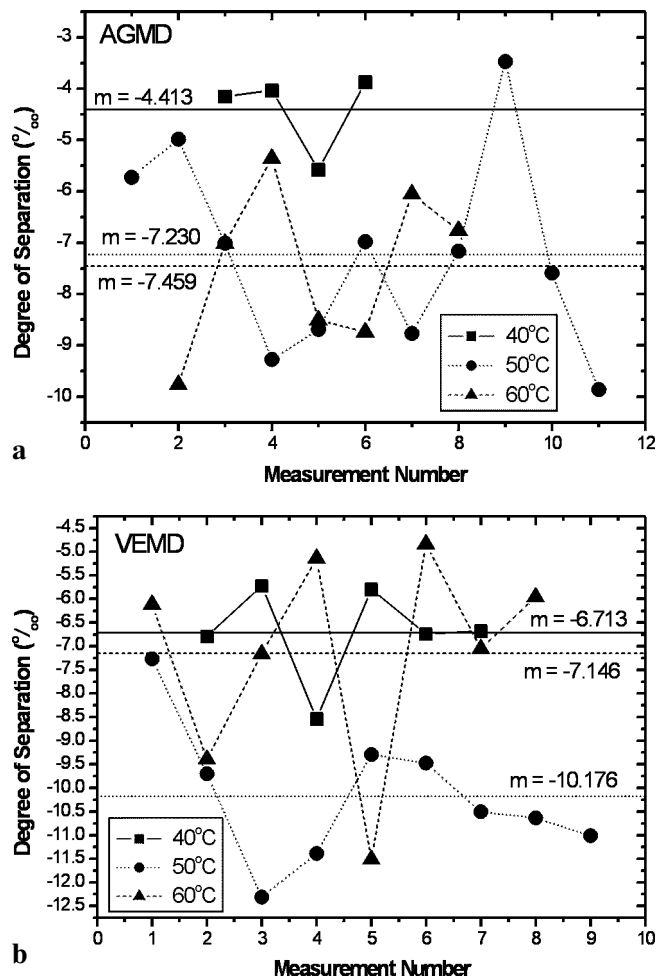


Fig. 5. Degrees of oxygen isotope separation for a hydrophobic PTFE membrane for (a) AGMD and (b) VEMD without heat exchange funnel.

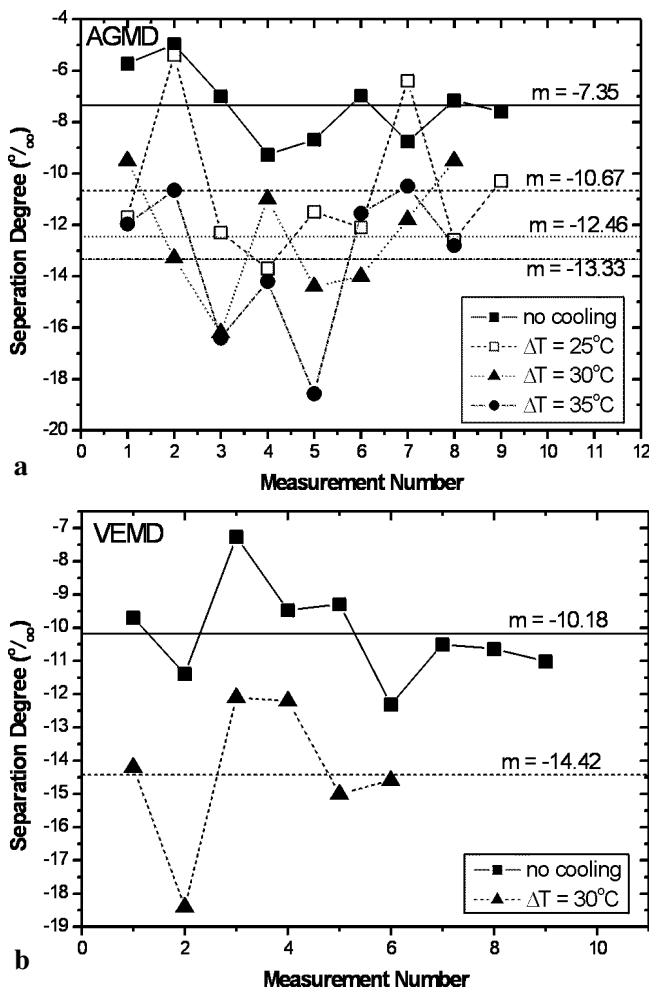


Fig. 6. Degrees of oxygen isotope separation for a hydrophobic PTFE membrane for (a) AGMD and (b) VEMD at $T_w = 50^\circ\text{C}$ with heat exchange funnel cooling.

shown in Fig. 2. Since air is initially filled into the membrane pores at the atmospheric pressure for AGMD, the mean free path of the water molecules in this case is much smaller than the pore diameter ($\sim 0.2 \mu\text{m}$) for any water vapor temperature because of the high total pressure. Hence, the bulk type of the water vapor flow in the pores should be considered. In this case, isotope separation can only be determined by the difference of the equilibrium vapor pressure of the isotopic water. This matches well with the experimental results in Fig. 4a except for the 40°C case. The isotope separation coefficients for a conventional fractional distillation of water which uses the equilibrium vapor pressure difference are 1.003 (110°C) \sim 1.008 (30°C) depending on the process temperatures [7]. Separation effects by the water vapor pressure difference in general increase as the water vapor temperature decreases. The MD experiments, on the other hand, show a lower separation effect at a lower temperature ($T_w = 40^\circ\text{C}$). This may be due to the smaller temperature gradient applied to the membrane surface for the 40°C case, because the processing water temperature is closer to the ambient temperature than the 50°C and 60°C cases. These show that the separation effects of MD depend not only on the equilibrium vapor pressure difference, but also on the temperature gradient applied to the membrane surfaces, which change the diffusion characteristics of the isotopic water vapor.

For VEMD, slightly higher separation effects than AGMD are observed, while the VEMD 60°C case shows lower separation effects than that for the VEMD 50°C case. When the water temperature is $\sim 60^\circ\text{C}$ for VEMD, this may be because the realistic λ is smaller than the pore diameter because of the shape of the pores even though the calculated λ of the water vapor at that temperature is slightly longer than the pore diameter. Hence, the separation effects for the VEMD 60°C may not be bigger than AGMD even though no air molecules exist in the pores in the same conditions. Clearly, the effect of oxygen isotope separation of MD is much bigger than that of the conventional water distillation process. Also the isotope separation effects of MD increase as the temperature gradient applied to membrane surface increases for both AGMD and VEMD.

Conclusions

By using AGMD and VEMD under various temperature conditions, water vapor permeation characteristics of a hydrophobic PTFE membrane based on the equilibrium vapor pressure were measured. As the temperature of the processing water and the membrane interfacial temperature gradient increase, the permeation flux of the water vapor increases due to an increase of the equilibrium vapor pressure and an increase of the membrane interfacial driving force. The permeation flux also increases significantly when the membrane interfacial pressure gradient increases for the VEMD case. Oxygen isotope separation of a hydrophobic PTFE membrane caused by the different equilibrium vapor pressures and additional differentiated water vapor pore transports between the isotopic water vapors was resulted. For both AGMD and VEMD, oxygen isotope separation depends on the processing water temperature and more importantly on the membrane interfacial temperature gradient.

Even though, oxygen isotope separation and the permeation flux for VEMD is slightly higher than AGMD, the latter may be more efficient from the system's operational point of view. Consequently, for the MD process, it is important to find the optimum conditions between the experimental parameters including the permeation flux, isotope separation coefficient, and temperature gradient, while the permeation cell is being operated efficiently.

Acknowledgment This work has been supported by a grant No M2-0305-01-005 from the Mid-Long Term Nuclear Energy Research Programme operated by the Ministry of Science and Technology in the Republic of Korea.

References

1. Chmielewski AG, Zakrzewska-Trznadel G, Miljević NR, Van Hook WA (1991) Investigation of the separation factor between light and heavy water in the liquid/vapor membrane permeation process. *J Membr Sci* 55:257–262
2. Chmielewski AG, Zakrzewska-Trznadel G, Miljević NR, Van Hook WA (1991) $^{16}\text{O}/^{18}\text{O}$ and H/D separation of water through a hydrophobic membrane. *J Membr Sci* 60:319–329
3. Chmielewski AG, Zakrzewska-Trznadel G, Miljević NR, Van Hook WA (1995) Membrane distillation employed for

- separation of water isotopic compounds. *Sep Sci Technol* 30;7/9:1653–1667
4. Chmielewski AG, Zakrzewska-Trznadel G, Miljević NR, Van Hook WA (1997) Multistage process of deuterium and heavy oxygen enrichment by membrane distillation. *Sep Sci Technol* 32;1/4:527–539
 5. Kerstel ERTh, Gagliardi G, Gianfrani L, Meijer HAJ, van Trigt R, Ramaker R (2002) Determination of the $^2\text{H}/^1\text{H}$, $^{17}\text{O}/^{16}\text{O}$, and $^{18}\text{O}/^{16}\text{O}$ isotope ratios in water by means of tunable diode laser spectroscopy at 1.39 μm . *Spectrochim Acta A* 58:2389–2396
 6. Kim J, Park SE, Kim TS, Jeong DY, Ko KH, Park KB (2003) Separation characteristics of oxygen isotopes with hydrophobic PTFE membranes. *Membrane Journal* 13;3:154–161 (in Korean)
 7. Krell E (1963) *Handbook of laboratory distillation*. Elsevier Publishing Co., London
 8. Park SE, Jeong DY, Kim J, Ko KH, Jung EC, Kim CJ (2003) Measurement of oxygen isotope ratios using tunable diode laser absorption spectroscopy. In: *Proc of the CLEO/Pacific Rim 2003. The 5th Pacific Rim Conf on Lasers and Electron Optics*, December 15–19, 2003, Taipei, Taiwan 1:241
 9. Van Hook WA, Chmielewski AG, Zakrzewska-Trznadel G, Miljević NR (1991) Method of enrichment of oxygen-18 in natural water. U S Patent 5,057,225, October 15, 1991